HHS Public Access

Author manuscript

J Control Release. Author manuscript; available in PMC 2022 April 14.

Published in final edited form as:

J Control Release. 2021 February 10; 330: 1118–1129. doi:10.1016/j.jconrel.2020.11.017.

Nanoparticle Delivery Improves the Pharmacokinetic Properties of Cyclic Dinucleotide STING Agonists to Open a Therapeutic Window for Intravenous Administration

Mohamed Wehbe[1], **Lihong Wang-Bishop**[1], **Kyle W. Becker**[1], **Daniel Shae**[1], **Jessalyn J. Baljon**[2], **Xinyi He**[1], **Plamen Christov**[3], **Kelli L. Boyd**[4,5], **Justin M. Balko**[6,7], **John T. Wilson**[1,2,3,5,7]

[1]Department of Chemical and Biomolecular Engineering, Vanderbilt University, Nashville, TN, 37232

[2]Department of Biomedical Engineering, Vanderbilt University, Nashville, TN, 37232, United States

[3]Vanderbilt Institute of Chemical Biology, Vanderbilt University, Nashville, TN, 37232, United States

[4]Department of Pathology, Microbiology, and Immunology, Vanderbilt University Medical Center, Nashville, Tennessee 37232, United States

[5]Vanderbilt Institute for Infection, Immunology, and Inflammation, Vanderbilt University Medical Center, Nashville, Tennessee 37232, United States

[6]Department of Medicine, Vanderbilt University Medical Center, Nashville, TN, 37232, United States

[7]Vanderbilt Ingram Cancer Center, Nashville, TN, 37232

Abstract

The stimulator of interferon genes (STING) pathway plays an important role in the immune surveillance of cancer and, accordingly, agonists of STING signaling have recently emerged as promising therapeutics for remodeling of the immunosuppressive tumor microenvironment (TME) and enhancing response rates to immune checkpoint inhibitors. 2′3’-cyclic guanosine monophosphate–adenosine monophosphate (2′3’-cGAMP) is the endogenous ligand for STING, but is rapidly metabolized and poorly membrane permeable, restricting its use to intratumoral administration. Nanoencapsulation has been shown to allow for systemic administration of cGAMP and other cyclic dinucleotides (CDN), but little is known about how nanocarriers affect important pharmacological properties that impact the efficacy and safety of CDNs. Using STING-activating nanoparticles (STING-NPs) – a polymersome platform designed to enhance cGAMP delivery – we investigate the pharmacokinetic (PK)-pharmacodynamic (PD) relationships that underlie the ability of intravenously (i.v.) administered STING-NPs to induce STING activation and inhibit tumor growth. First, we demonstrate that nanoencapsulation improves the half-life of encapsulated cGAMP by 40-fold, allowing for sufficient accumulation of cGAMP in tumors

(Corresponding author) Contact information for John T. Wilson: john.wilson@vanderbilt.edu, Tel: 615-322-6406; Fax: 615-343-7951.

and activation of the STING pathway in the TME as assessed by western blot analysis and gene expression profiling. Nanoparticle delivery also changes the biodistribution profile, resulting in increased cGAMP accumulation and STING activation in the liver and spleen, which we identify as dose limiting organs. As a consequence of STING activation in tumors, i.v. administered STING-NPs reprogram the TME towards a more immunogenic antitumor milieu, characterized by an influx of >20-fold more $CD4^+$ and $CD8^+$ T-cells. Consequently, STING-NPs increased response rates to αPD-L1 antibodies, resulting in significant improvements in median survival time in a B16-F10 melanoma model. Additionally, we confirmed STING-NP monotherapy in an additional melanoma (YUMM1.7) and breast adenocarcinoma (E0771) model leading to >50% and 80% reduction in tumor burden, respectively, and significant increases in median survival time. Collectively, this work provides an examination of the PK-PD relationship governing STING activation upon systemic delivery using STING-NPs, providing insight for future optimization for nanoparticle-based STING agonists and other immunomodulating nanomedicines.

Graphical Abstract:

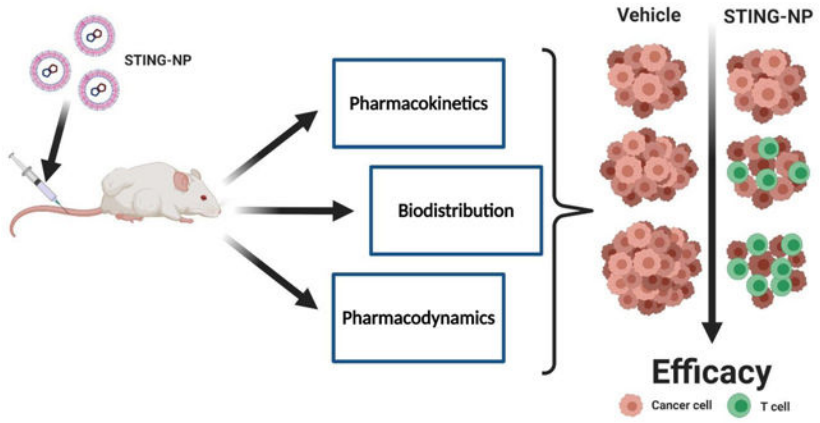

Keywords

cGAS-STING; pharmacokinetics; polymersome; nanoparticle; cGAMP; immunotherapy; immune checkpoint blockade

Introduction:

Recent advances in immunotherapy have transformed cancer medicine. The success of monoclonal antibody immune checkpoint inhibitors (ICIs) that enhance the function of anti-tumor T lymphocytes has garnered significant attention due to their ability to generate robust and durable responses in some patients [1–3]. Unfortunately, this is not ubiquitous across tumors or cancer types; for example, in advanced metastatic melanoma, where ICIs have had the most dramatic clinical impact, only a minority (10–40%) of patients exhibit durable responses to single-agent ICI [1, 4]. The most predictive biomarker for efficacy of ICIs is the immune contexture of the tumor microenvironment (TME) wherein tumors that are phenotypically T-cell inflamed, or “hot”, tend to respond substantially better to ICIs than those that are immunologically “cold” and lack significant T-cell infiltration [5–7]. One

of the hallmarks of cancer is the establishment of an immunosuppressive environment that allows for immune escape; therefore, it stands to reason that many tumors will be of a “cold” phenotype, especially when diagnosed at later stages when an immunosuppressive network has already been established [8].

The ability to shift the TME from an immunologically “cold” to “hot” phenotype has been the focus of significant research as a strategy to improve responses to ICIs [9, 10]. Amongst a growing myriad of strategies, the use of molecularly-defined pattern recognition receptor (PRR) agonists is being explored as a promising approach to increasing the immunogenicity of the TME [11, 12]. Activation of PRR signaling stimulates an innate immune response capable of initiating and propagating anti-tumor immunity through multiple mechanisms, including repolarization of immunosuppressive myeloid cells, generation of T cell chemokine gradients, and enhancing tumor antigen presentation and subsequent T cell activation. Ligands for a number of different PRRs have been pursued with variable degrees of clinical success. For example, the Toll-like Receptor (TLR) 9 agonist CpG-B oligonucleotide [13] and TLR3 agonist poly(IC) [14] have shown success in phase I/II clinical trials when administered intratumorally. More recently, activation of the stimulator of interferon genes (STING) pathway has also shown great promise for increasing tumor immunogenicity in pre-clinical tumor models. 2′3’-cyclic guanosine monophosphate–adenosine monophosphate (2′3’-cGAMP) is the endogenous ligand for STING but other natural and synthetic cyclic dinucleotides (CDN) are active and their ability to stimulate antitumor innate immunity has been explored [15–17]. As a class of therapeutics, CDNs require intracellular delivery to bind the STING protein localized on the cytosolic face of the endoplasmic reticulum (ER). This challenge is exacerbated by their poor membrane permeability, degradation by nucleases, and short half-life which results in minimal accumulation in tumor sites or lymphoid organs [18–20]. These drug delivery barriers have limited the use of CDNs to local intratumoral (i.t.) therapy. While this administration route cannot be easily adapted for all patients or cancer types, it provides a direct approach to investigate the safety and pharmacodynamics of CDNs and the effects of STING activation on antitumor immunity. Importantly, in mouse tumor models, i.t. delivery of STING agonists can elicit a systemic tumor antigen-specific T cell response capable of inhibiting the growth of distal, untreated tumors (i.e., abscopal effect) [17, 21] and generating immune memory to prevent disease recurrence [22, 23]. Aduro Biotech and Merck have developed synthetic CDNs (ADU-S100 and MK-1454, respectively) with chemical modifications that improve cell permeability and stability, and have advanced these molecules into Phase I/II clinical trials of i.t. administration into metastatic lesions [24, 25]. However, many patients are ineligible due to poor accessibility of their tumors for i.t. administration [25], and, while improving, clinical evidence of abscopal responses still remains largely anecdotal [26, 27]. Unfortunately, while newer generations of CDNs have improved stability and cell permeability, they have not been demonstrated to be effective when administered systemically, which may be a necessity for cancer patients with inaccessible tumors and/or advanced, metastatic disease. Thus, developing, understanding, and optimizing strategies to enhance systemic CDN delivery is a priority of high clinical significance.

To address this challenge, nanotechnology is being leveraged to formulate CDNs for systemic (i.v.) delivery. The use of liposomal carriers has been most commonly employed, with several groups exploiting the charge-charge interaction between a cationic lipid (e.g., DOTAP, YSK05) and anionic CDN to improve encapsulation efficiencies and enhance cytosolic delivery [22, 28–30]. Our group has recently described the development of endosome-destabilizing polymer vesicles (polymersomes) that enhance the cellular uptake and cytosolic delivery of cGAMP [31]. Referred to as STING-activating nanoparticles (STING-NP), the particles have an aqueous core for CDN loading and a vesicle membrane comprising amphiphilic diblock copolymer chains with pH-responsive, endosomal membrane-destabilizing activity, a design that increases the biological potency of cGAMP by 2–3 orders of magnitude. Importantly, particles are also surface charge neutral with a dense 2kDa PEG corona, a design that enables i.v. administration and dramatically enhances the therapeutic efficacy of cGAMP. Yet, in our previous work, and in other reports that have deployed nanoparticle delivery of CDNs, the focus has been primarily on demonstration of efficacy, with minimal investigation into how nanocarriers modulate key pharmacological properties of CDNs. Thus, this work aims to determine how the pharmacokinetics (PK) and biodistribution of STING-activating nanomedicines, which are rapidly expanding in use, impact antitumor immunity, therapeutic efficacy, and toxicity. Such mechanistic insight linking the pharmacological properties of CDNs to antitumor efficacy will be critical to the rational development of next generation carrier technologies for STING agonists with potential to also inform nanoparticle design criteria that are broadly applicable to other types of innate immune agonists.

Materials and Methods:

Polymer Synthesis:

Poly[(ethylene glycol)-*block*-[(2-diethylaminoethyl methacrylate)-*co*-(butyl methacrylate)-*co*-(pyridyl disulfide ethyl methacrylate)]] polymers were synthesized via reversible addition-fragmentation chain transfer (RAFT) polymerization as previously described [31] (Polymer Characterization Figure S1). Polymer was labelled through reduction of PDSMA groups using TCEP and reaction with Cy5-PEG_4-maleimide (Click Chemistry Tools) at 25°C for 2 hours. The polymer was then dialyzed using SnakeSkin™ dialysis tubing (3.5K MWCO, Thermofisher) against water twice for 48 h and lyophilized. This was then mixed with native polymer at a ratio of 1:5 (labelled:unlabelled), dissolved in a minimal volume of acetone, and precipitated in cold (−20°C) pentane. The precipitated polymer was then dried in a vacuum oven for 48 h.

STING-NP Formulation:

STING-NPs were formulated as previously described [31]. Briefly, the synthesized polymer was dissolved in ethanol (1000 mg/mL) and heated to 37°C for 20 mins. To this solution an equivalent volume, relative to the amount of ethanol used, of 50 mg/mL concentrated 2',3' cyclic GMP-AMP (cGAMP) or ^{3}H-cGAMP (Moravek) solution in DI water was added, mixed, and allowed to equilibrate at 37°C for 1 hr. cGAMP was synthesized in house as described previously [31]. The resultant gel was diluted in DI water and sonicated at 40°C for at least 2 hours to disperse the nanoparticles. Finally, 0.5 molar equivalents

of dithiothreitol (DTT), relative to the total number of pyridyl disulfide moieties in the formulation, were added to crosslink polymer chains. Centrifugal filtration (Amicon, 3kDa MWCO) was used to remove any unencapsulated drug and byproducts of the crosslinking reaction to yield STING-NPs. The resultant nanoparticles were analyzed by dynamic light scattering (Malvern Zetasizer Nano ZS) and the amount of entrapped cGAMP was measured using normal phase HPLC as previously described [32].

In vivo analysis of toxicity:

6–8 week old female C57BL/6 mice were treated intravenously with vehicle (PBS; n=3) or STING-NPs (20 or 10 μg, n=5) for three injections three days apart. Body weight and signs of toxicity were assessed daily for 10 days. On day 10 (24 h after final treatment), mice were euthanized and organs (liver, lung, kidney, spleen, pancreas, heart, sternum and, brain) were harvested and fixed in 10% formalin for pathology. Organs were embedded in paraffin, sectioned at 5 μm, and stained with hematoxylin and eosin (H&E). Sections were evaluated by an experienced veterinary pathologist blinded to the composition of the groups. For analysis of blood chemistry, blood was collected, allowed to clot at room temperature, centrifuged at 1000xg for 15 mins, and serum was analyzed on an Alfa Wasserman ACE Alera in the Vanderbilt University Medical Center Translational Pathology Shared Resource (VUMC TPSR).

Cell Culture:

B16-F10 cells were obtained from American Type Culture Collection (ATCC) (Manassas, Virginia). E0771 and YUMM1.7 cells were gifted from Drs. Justin Balko (Vanderbilt Univeristy) and Marcus Bosenberg (Yale University) respectively. B16-F10 cells were maintained in Dulbecco's modified Eagle's medium (Gibco) supplemented with 10% fetal bovine serum (FBS; Invitrogen, Carlsbad, California), 100 U ml^{-1} penicillin (Gibco) and, 100 μg ml^{-1} streptomycin (Gibco). E0771 cells were maintained in RPMI 1640 medium (Gibco) with 10 mM HEPES and supplemented with 10% FBS (Invitrogen, Carlsbad, California) 100 U ml^{-1} penicillin (Gibco) and, 100 μg ml^{-1} streptomycin (Gibco). YUMM1.7 cells were maintained in DMEM/F12 (1:1) (Gibco) supplemented with 2 mM L-glutamine, 15 mM HEPES, 10% FBS (Invitrogen, Carlsbad, California), 100 U ml^{-1} penicillin (Gibco), 100 μg ml^{-1} streptomycin (Gibco), and, 1× non-essential amino acids (Cellgro). Cells were passaged when confluency reached 70–90% using 0.05% trypsin (Gibco) for B16-F10 and E0771 cells or Accutase (Gibco) for YUMM1.7.

Ethics Statement:

All studies using animals were completed under an Animal Care Protocol (M1800155) approved by the Vanderbilt University Institutional Animal Care and Use Committee (IACUC). Animal health assessments were completed using standard operating procedures approved by Vanderbilt University IACUC.

Subcutaneous Tumor Models:

B16-F10 (5×10^5) or E0771 (5×10^5) cells were suspended in 100 μL PBS and subcutaneously injected into the right flank region of 6–7-week-old female C57BL/6 mice

(The Jackson Laboratory, Bar Harbor, ME). Similarly, YUMM1.7 (1×10^6) cells were inoculated in 7-week-old male C57BL/6 mice. Established B16-F10 (75 mm^3) tumors were treated with vehicle (PBS), STING-NP (10 μg, every 3 days for 3 injections) intravenously and/or αPD-L1 (100 μg, every 3 days for 5 injections, BioXcell, West Lebanon NH) intraperitoneally. For monotherapy studies, established YUMM1.7 (~50 mm^3) and E0771 (~75 mm^3) tumors were treated with vehicle or STING-NP (10 μg, every 3 days for 3 injections) intravenously. Tumor volume was measured every 3 days via caliper measurements, and volumes were calculated using ($V_{tumor} = L \times W^2 \times 0.5$, in which V_{tumor} is tumor volume, L is tumor length, and W is tumor width). Mice were euthanized by carbon dioxide asphyxiation when tumor volume reached >1500 mm^3.

Analysis of pharmacokinetics and biodistribution:

cGAMP Quantification: STING-NPs were formulated as described above using ^{3}H-cGAMP. 6–7-week-old female C57BL/6 mice were inoculated with B16-F10 melanoma cells (5×10^5) subcutaneously into the right flank region. When tumors reached a volume of 100–200 mm^3, mice were injected i.v. (100 μL per mouse) with free ^{3}H-cGAMP (~20 μg, 1 μCi) or STING-NPs (~10 μg, 1 μCi) containing ^{3}H-cGAMP and euthanized at 0.25, 1, 4, and 8 hours post injection. Whole blood was collected in EDTA-coated microfuge tubes through cardiac puncture and plasma was obtained by centrifugation for 20 mins at 2000 xg. Liver, lung, kidney, spleen, and tumor were removed and placed in pre-weighed scintillation vials at −80°C until processing. To obtain plasma concentrations at 0.083 h, mice were injected via tail vein and blood was obtained through submandibular bleed.

Whole livers were made into 30% homogenates in a known amount of water using an Ultra Turrax T25 tissue homogenizer (IKA, Wilmington NC). Aliquots (in triplicate) of 200 μL homogenate were transferred to scintillation vials. All organs and liver homogenates were mixed with 500 μL Solvable (PerkinElmer, Waltham MA) and incubated overnight at 50°C. The dissolved tissues were allowed to cool for 1 h prior to the addition of 50 μL EDTA (500 mM, pH 8) and 300 μL H_2O_2 (added 100 μL at a time) before reheating to 50°C for 20 mins. This was cooled to RT, mixed with 5 mL Pico-Fluor Plus (PerkinElmer, Waltham MA) scintillation cocktail, and was stored in the dark until analysis. Plasma was mixed directly with scintillation cocktail and all samples were read on a Liquid Scintillation Counter (Packard 1900TR Liquid Scintillation Analyzer).

Polymer Quantification: 6–7-week-old female C57BL/6 mice were inoculated with B16-F10 tumor cells (5×10^5) subcutaneously into the right flank region. When tumors reached a volume of 100–200 mm^3 mice were injected i.v with empty Cy5-labelled STING-NPs. At 0.5, 1, 4, and 24 h post-injection whole blood was collected in EDTA-coated microfuge tubes and plasma was obtained by centrifugation for 20 mins at 2000 xg. Liver, lung, kidney, spleen and tumor were removed and placed on ice for IVIS imaging. To obtain plasma concentrations at 0.5 hr, mice were injected and blood was obtained through submandibular bleed. To quantify the amount of polymer in plasma, a standard curve was made using doped (1:5) Cy5-labelled to unlabeled polymer in methanol. The plasma was mixed with methanol and centrifuged at 1000 xg for 5 mins at 4°C. The supernatant was read on a Synergy H1 (Biotek, Winooski, VT) plate reader.

In vitro nanoparticle release assays:

cGAMP Leakage from Nanoparticle: 3H-cGAMP was loaded into polymerosomes as described above and added to slide-a-lyzer 20 KDa cut-off dialysis filter (thermofisher). The nanoparticles were dialyzed against PBS (pH 7.4) at 37^{o}C for 24 hours. At indicated timepoints a 50 uL aliquot of particle was added to a glass scintillation vial. The ^{3}H-cGAMP content in the nanoparticles was measured using scintillation counting and percent release was calculated by comparing to the zero timepoint concentration.

Activity of STING-NPs in Raw-Blue ISG cells: STING-NPs were incubated with PBS (pH 7.4) at 37oC for 0, 3, 8 or 24 hours. The activity of these nanoparticles to induce responses in a RAW-Blue ISG cell line was evaluated as per manufactures instructions using Synergy H1 (Biotek, Winooski, VT) plate reader.

Quantification of plasma interferon β:

Plasma concentration of mIFNβ at 1, 4, 8, 24, and 48 h post-injection of cGAMP or STING-NPs was quantified using the LumiKine™ Xpress mIFN-β 2.0 (Invivogen) as per manufacturer's instructions.

Quantification of plasma pro-inflammatory cytokines:

Plasma concentration of IFN-α, IFNγ, IL-6 and TNFα at 4, and 24 h post-injection of Vehicle, Empty Nanoparticle, cGAMP or STING-NPs was quantified using a Legendplex™ custom mouse cytokine panel (Biolegend) as per manufacturer's instructions.

Western blot analysis of tumors:

Vehicle and STING-NP treated B16-F10 tumors were homogenized using a TissueLyser II (Qiagen) in RIPA lysis buffer (Santa Cruz). The protein concentration was determined using a BCA assay (Thermo Scientific, Waltham, Massachusetts), samples were run on a SDS-PAGE and transferred onto a nitrocellulose membrane using a semi-dry transfer protocol (Bio-Rad laboratories, Hercules, California). Membranes were washed and incubated with primary antibody (p-IRF3, IRF3, STING, and β-actin) at 4^{o}C overnight, followed by blotting with HRP-conjugated secondary antibodies (Promega). The protein bands were obtained with the ChemiDoc XRS+system (Bio-Rad) using an immobile western Chemiluminescent HRP Substrate Kit (Millipore Sigma, Billerica, Massachusetts). Protein loading was normalized for equal amounts of actin; representative images from at least 3 independent experiments are shown.

Quantitative real-time PCR:

C57BL/6 mice bearing 100–200 mm^{3} B16-F10 tumors were treated with STING-NPs (10 μg, intravenously) and euthanized at 1, 4, and 8 h post-injection. Liver, lung, kidney, spleen, tumor, and draining and contralateral lymph nodes were collected and snap frozen. Organs were homogenized using TissueLyser II (Qiagen) and total RNA was isolated using the RNeasy Mini kit (Qiagen, Germantown, MD). Total RNA (1 μg) was reverse transcribed by an iScript cDNA synthesis kit (Bio-Rad) and qPCR was performed using a TaqMan Mastermix kit (Thermo Fisher Scientific) as per manufacturer's instructions. All organs

were examined for *Ifnb1* gene expression. Lymph nodes and tumor expression of CXCl10 was examined. Additionally, tumor lysates were analyzed for *Tnfa* and *Il12b* expression. This was all compared to basal levels of *Hmbs* expression. The TaqMan gene expression primers were purchased from ThermoFisher Scientific (Waltham, Massachusetts): mouse *Tnfa* (Mm00443258_m1); mouse *Ifnb1* (Mm00439552_s1); *Cxcl10* (Mm00445235_m 1); mouse *Il12b* (Mm00434174_m1) and mouse *Hmbs* (Mm01143545_m1).

Flow Cytometric Analysis of Tumor Microenvironment:

C57BL/6 mice bearing 100–200 mm^3 B16-F10 tumors were treated with STING-NPs (10 μg, intravenously) or vehicle (PBS) every 3 days for three total injections. Mice were euthanized 24 h after final treatment Tumors were harvested, weighed, and placed on ice. The tumors were mechanically dissociated using an OctoMACS separator (Miltenyi) and digested in RPMI 1640 containing 125 μg/mL deoxyribonuclease I and 500 μg/mL collagenase III for 30 mins at 37ºC. The cell suspension was strained through a cell strainer (40 μm), red blood cells were lysed using ACK lysis buffer (Gibco). Cells were then resuspended in flow buffer (5% BSA in PBS), counted and stained with the following flow panels (antibodies obtained from Biolegend). *Tumor Microenvironment:* Panel I: FITC-αCD45 (30-F11), APC-αCD3 (17A2), APC/Cy7αCD4 (RM4–5), PE/Cy5-αCD8α (53–6.7) and DAPI. Panels II: FITC-αCD45 (30/F11), PE/Cy5-αCD11b (M1/70), APC/Cy7–αF4/80 (BM8), BV711-αMHC-II(M5/114.15.2),PE-αNK1.1(PK136), BV510-Ly6G (1A8), APC-Ly6C (HK1.4) and DAPI (Millipore Sigma, Billerica, Massachusetts). Cells were then washed twice, suspended in flow buffer containing Accu-chek counting beads and analyzed on a BD LSR II flow cytometer. All flow cytometry data were analyzed using FlowJo software (version 10; Tree Star; https://www.flowjo.com/solutions/flowjo). Representative flow cytometry plots and gating schemes are shown in Figures S2 and S3.

Flow Cytometric Analysis of Nanoparticle Uptake:

C57BL/6 mice bearing 100–200 mm^3 B16-F10 tumors were treated once with Cy5-STING-NPs. Mice were euthanized 24 h after final treatment, tumors were harvested, weighed, and placed on ice. The tumors were mechanically dissociated, digested, and strained into single cell suspension as described above. Cells were then resuspended in flow buffer (5% BSA in PBS), counted, and stained with the following flow panels (antibodies obtained from Biolegend). Panels I: FITC-αCD45 (30-F11), PE/Cy5-αCD11b (M1/70), APC/Cy7–αF4/80 (BM8), PE/Cy7- αNK1.1, BV510-Ly6C (HK1.4) and DAPI. Panel II: APC/Cy7-αMHC-II (M5/114.15.2), PE –αCD11c (N418), PE/Cy7-αCD3 (17A2), BV510-Ly6C (HK1.4) and DAPI (Millipore Sigma, Billerica, Massachusetts). Cells were then washed twice, suspended in flow buffer containing Accu-chek counting beads, and analyzed on a BD LSR II flow cytometer. Representative flow cytometry plots and gating schemes are shown in Figure S4.

Statistical Analysis:

The data were plotted using Prism 8 (Graphpad) software as the mean ± SD unless otherwise stated in the figure legend. For pharmacokinetic experiments, the data were analyzed using PK solutions software. Blood chemistry and immune cell infiltration were compared by Student’s t-test. Biodistribution, qPCR, and tumor volume significance were examined through a one-way ANOVA followed by Tukey’s adjustment for multiple comparisons.

A log-rank test was used to compare Kaplan-Meyer survival data. *P*-values <0.05 were considered significant in these studies. All flow cytometry data were analyzed using FlowJo software (version 10; Tree Star; https://www.flowjo.com/solutions/flowjo).

Results:

Splenic and Hepatic Toxicities Limit the Therapeutic Window of STING-NPs:

The vast majority of studies evaluating CDN STING agonists for cancer therapy, including in current clinical trials, have focused on i.t. administration due, in part, to the ability to generate a sufficiently high i.t. dose while also increasing the safety profile [24, 25, 33]. Nanocarriers can significantly change the biological activity and distribution of drug cargo with important effects on toxicity; therefore, we first sought to determine a maximum tolerated dose (MTD) for i.v. administered STING-NPs and to establish correlates between dose and markers of systemic toxicity. The MTD of STING-NPs was determined in non-tumor bearing, female C57BL/6 mice using a dose of 10 or 20 μg cGAMP administered every 3 days (Figure 1A), and mouse weight and survival was measured over 10 days (Figure 1B,C). Administration of STING-NPs at 20 μg of cGAMP resulted in >15% weight loss within the first 1–2 days following administration and 3/5 mice did not survive the full course of treatment. In contrast, a dose of 10 μg resulted in only a transient weight loss of <10% and all mice survived the three-injection treatment regimen. One day following the last administration, organs (liver, spleen, lungs, heart, kidney, and brain) were isolated, fixed, and paraffin embedded for pathology. For surviving mice treated with 20 μg of STING-NPs, hepatic necrosis and marked apoptosis in the splenic white and red pulp was observed, but all other organs (lung, kidney, heart and brain) were found to have unremarkable changes when compared to healthy mouse tissue. By contrast, mice treated with 10 μg STING-NP did not show any signs of toxicity at the organ level (Figure 1C). Blood chemistry was evaluated 24 hours after the final dose; alanine aminotransferase (ALT), aspartate transaminase (AST), creatinine, and glucose levels were not statistically different from treatment naïve control mice. Blood urea nitrogen (BUN) and total protein, while largely in the normal range for mouse blood chemistry, were slightly elevated above vehicle treatment (Figure 1D). Additionally, histopathology revealed no indication of damage to the endothelium or vascular leakage as evidenced by a lack of edema and fibrin formation around the vessel lumen and no signs of vasculitis or perivascultisis in any of the tissues. In aggregate, these results suggest that the liver and spleen are dose limiting organs for systemically administered STING-NPs and identify an MTD of 10 μg cGAMP when administered using a therapeutic three injection regimen.

Nanoparticle Encapsulation of cGAMP Increases Circulation Lifetime:

Cyclic GMP-AMP synthase (cGAS) produces 2’3’-cGAMP cytosolically in response to microbial and self-DNA which in turn binds to STING localized on the ER membrane. Hence, endogenously produced cGAMP acts intracellularly and locally and is therefore not limited by the physiochemical properties that hinder its translation and utility as a drug product. By contrast, STING-NPs, and other nanoparticle delivery systems, enhance the delivery and activity of extracellular, exogenous cGAMP to cells and organs upon systemic administration. However, there has been no investigation into how delivery systems impact

CDN pharmacokinetics and biodistribution, studies that are needed to better understand mechanisms of action and toxicity that can also inform the development of optimized systems. Thus, we assessed the circulation lifetime of cGAMP and polymer in C57BL/6 mice (Figure 2A/B). To measure the pharmacokinetic profile and organ accumulation of cGAMP, mice were injected with STING-NPs loaded with ^{3}H-cGAMP or soluble ^{3}H-cGAMP (20 μg free cGAMP or 10 μg STING-NP) prepared from a 50 mg/mL cGAMP stock solution doped with ^{3}H-cGAMP. When injected intravenously, cGAMP has a half-life of approximately 2 mins (Figure 2A), resulting in poor organ accumulation, which, in addition to its poor cellular permeability, results in little to no STING activation *in vivo*. STING-NPs improve the elimination half-life of cGAMP to 1.3 h, a 40-fold increase, and enhance the $AUC_{0\text{-}inf}$ by 6.5-fold (Table 1). This increase in circulation time and exposure results in increased organ and tumor tissue accumulation of cGAMP. Unsurprisingly, the majority of the injected dose (~15%) was found to accumulate in the liver (Figure 2C) between 0.25–4 h and was largely cleared by 8 h. While free cGAMP does not accumulate in the tumor tissue, when it is administered using STING-NPs 1–3% of the injected dose was found in B16-F10 tumors between 0.25–4 h. cGAMP administered with STING-NPs also accumulates in organs besides the liver (e.g., spleen, kidney, and lung), only the spleen was noted during pathologic analysis as an organ of interest. The maximum percent injected dose for this tissue is only ~1.5%, but the spleen also has a high density of immune cells that may be more sensitive (human protein atlas) [34] to STING agonists and this likely contributes to the pathology observed in the spleen at higher cGAMP doses [35–37].

To obtain a more complete understanding of cGAMP distribution phenomena, polymersomes were prepared using Cy5-labelled polymer chains and injected at a dose corresponding to 0.75 mg polymer per mouse (~37.5 mg/kg polymer). The half-life of the polymersome was estimated to be 6.4 h, longer than that observed for cGAMP, potentially suggesting a burst release or leakage of cGAMP from the particle within 4 hours (Figure 2B), a common limitation of vesicular drug carriers [38–41]. The particle biodistribution was also tracked by fluorescent imaging of organs using IVIS (Figure 2D). Particles accumulated primarily in the liver and spleen (5–10 fold over baseline), whereas minimal uptake was observed in the lung and kidneys. We offer the caveat that caution must be taken in assigning quantitative relationships between cGAMP and polymer accumulation when two different analytical methods (e.g., scintillation counting and IVIS imaging) are employed owing to differential sensitivity, quantitative accuracy, and inherent limitations (e.g., tissue penetration).

STING-NPs stimulate a transient, systemic inflammatory response:

STING activation leads to the production of type I interferons (IFN-I), interferon stimulated genes (ISGs), and pro-inflammatory cytokines [42]. However, levels of STING and downstream signaling molecules (e.g., TBK1) vary considerably between tissues and, therefore, organ-level pharmacodynamics, as measured by the magnitude of STING activation, may not directly correlate with cGAMP biodistribution [34]. Therefore, B16-F10 tumor-bearing mice were treated with cGAMP or STING-NPs, and blood and major clearance organs were analyzed for IFN-I and other STING-driven cytokines. Plasma was analyzed for secreted IFNβ by ELISA. STING-NP treated mice were found to have a IFNβ

C_{max} of 15000 pg/mL at 4 hours post injection (Figure 3A) which returned to baseline levels by 24 h. The serum concentration of cytokines (IFN-α, IFNγ, IL-6 and TNFα) were also analyzed by cytokine bead array at 4 and 24 h post-injection (Figure S5), with similar trends observed. Additionally, i.v. administration of empty polymersomes and free cGAMP did not result in significant elevation of cytokine levels, further demonstrating that the response is STING-dependent and that packaging of cGAMP into polymersomes is critical to achieving *in vivo* activity. To determine the extent of STING activation in organs, qRT-PCR was used to quantify transcript levels of *Ifnb1* as a downstream marker. As expected, the liver and spleen showed the greatest increase in *Ifnb1* expression (Figure 3B), with the most significant elevation observed in the spleen, consistent with a high density of immune cells. The kidney showed a modest but statistically significant increase in *Ifnb1* over free cGAMP at 4 hours. Levels of *Ifnb1* in the lung were below background for both groups. In summary, these results further indicate that the liver and spleen are the organs limiting the MTD for STING-NPs and likely for other STING-activating nanoparticle formulations that are cleared by the reticuloendothelial system.

Systemic STING-NP Administration Remodels the Tumor Immune Microenvironment:

Systemic administration of STING agonists for cancer immunotherapy is suspected to require sufficient activation of STING signaling at tumor sites and/or in lymphoid tissue at well-tolerated doses. Therefore, we evaluated protein-level expression of STING, IRF3, and phospho-IRF3 (pIRF3) in B16-F10 tumors following intravenous injection of STING-NP or vehicle to confirm activation of the STING pathway (Figure 4A). The activation of the STING pathway in the tumor was further supported by qRT-PCR examining downstream genes (*Ifnb1*, *Cxcl10*, *Tnfa*, and *Il12*) at 1, 4, and 8 h (Figure 4B). All genes showed significant increases in expression by 4 h when compared to free cGAMP. As the tumor-draining lymph node (TDLN) is an important site of anti-tumor T cell priming and activation that is often also immunosuppressed [43], we also evaluated expression of *Ifnb* and *Cxcl10* in the inguinal LN (Figure 4C) and observed a significant increase in *Cxcl10* at 8 h, but no change in *Ifnb* levels, suggesting that i.v. administration of STING-NPs may also modestly increase STING signaling in the TDLN.

We next sought to determine the primary cell populations in the tumor that were passively targeted by STING-NPs, and, therefore, may be key cellular mediators of STING activation. To assess the extent of particle uptake by immune cells, mice were injected with Cy5-labeled polymersomes and the spleen, tumor, and TDLN were collected 24 hours post-injection, a timepoint where both carrier and cGAMP had cleared the circulation. In B16-F10 tumors, <5% of tumor-associated immune cells were found to have endocytosed i.v. administered particles (Figure 4D). While this represents a relatively small population of immune cells, this finding is also consistent with a number of previous reports investigating cellular uptake of i.v. administered NPs in tumors, and suggests that therapeutic benefit can be achieved through delivery to a relatively small subset of immune cells in the TME [44, 45]. Given their important role in priming of antitumor T cell responses, we also evaluated immunocellular uptake of polymersomes in the spleen and TDLN. Not surprisingly, and consistent with observed cGAMP distribution to the spleen, NPs were endocytosed by a high percentage of splenic macrophages and DCs. While beyond the scope of the current

work, this raises the possibility that STING-mediated activation of APCs in the spleen may support priming of antitumor T cells or that myeloid cells may potentially migrate from the spleen into tumors to exert antitumor functions [46]. Interestingly, we also observed a significant accumulation of NPs in dendritic cells in the tumor draining (inguinal) lymph node. Whether these represent DCs that have endocytosed NPs and migrated from the tumor into the LN or have captured NPs that distribute into LNs from the circulation or tumor site was not explored, but nonetheless may also play an important role in enhancing immune responses to tumor antigens. We note that this data pertains only to the cellular uptake of fluorescently-labeled polymer chains and, therefore, may not reflect the pattern or magnitude of cGAMP distribution amongst these same cell populations.

Finally, having demonstrated STING activation in the tumor, we then aimed to examine changes to the immunocellular profile of the TME upon administration of a three dose, therapeutic STING-NP regimen (Figure 4E/F). Most notably, a significant, >20-fold increase, in the numbers of $CD4^+$ and $CD8^+$ T-cells was observed, consistent with increased *Cxcl10* expression in tumors. Additionally, a slight increase in the number of $CD11c^+MHCII^+$ DCs was observed, while the number of $CD11b^+F4/80^+$ Mφ slightly decreased. Other immune cells ($CD11b^+Ly6C^+$ m-MDSCs and $CD45^+NK1.1^+$ NKs) showed no significant difference after treatment. Collectively, these data demonstrate that i.v. administered STING-NPs can dramatically enhance tumor T cell infiltration, therefore converting “cold” B16-F10 melanoma tumors to a T cell-inflamed TME.

Intravenous administration of STING-NPs reduces tumor burden in models of melanoma and breast cancer:

We next investigated the ability of STING-NPs to synergize with αPD-L1 immune checkpoint therapy in a B16-F10 melanoma model. In these studies, mice were treated with vehicle, αPD-L1 (100 μg, 5 treatments 3 days apart), STING-NP (10 μg, 3 treatments 3 days apart), or αPD-L1 and STING-NP (Figure 5A–D). By day 15 post-inoculation, STING-NP treated mice showed ~75% reduction in tumor burden in comparison to vehicle treated mice (Figure 5B,C). Additionally, mice treated with STING-NPs alone or in combination with αPD-L1 showed an increase in median survival time of 26 and 30 days, respectively (Figure 5D). The combination of STING-NP and αPD-L1 resulted in a significant increase in survival relative to either treatment alone (Figure 5D).

The work conducted to understand the PK-PD relationship for STING-NPs was performed in B16-F10 melanoma, a well-established model of a “cold” tumor that is non-responsive to ICI monotherapy. To validate that the efficacy of systemic STING-NP treatment translated to other murine tumor models we also evaluated STING-NP monotherapy at the MTD in YUMM1.7 (melanoma) and E0771 (breast cancer) models (Figure 5). We selected YUMM1.7 as another melanoma model since, like B16-F10, it is largely resistant to ICIs, but is BrafV600E, $Pten^{-/-}$, $Cdkn^{-/-}$ and has a low mutational load. Mice bearing YUMM1.7 (50 mm^3) tumors were treated with STING-NP, resulting in a >50% reduction in tumor volume on day 19 and a small, albeit significant, difference in survival. Finally, to demonstrate the efficacy of i.v. administered STING-NPs outside of melanoma, we also evaluated STING-NPs in a E0771 murine model of triple negative breast cancer. STING-NP

monotherapy in established E0771 tumors (75 mm^3) reduced tumor burden by 80% by day 20, and increased the median survival time from 22 to 33 days. Collectively, these studies demonstrate the efficacy of STING-NP monotherapy in mouse models of melanoma and breast cancer.

Discussion:

Identifying agents capable of remodeling the tumor microenvironment from “cold” (i.e., lacking T-cell infiltration) to “hot” (T-cell inflamed) phenotypes has rapidly emerged as a promising strategy for reversing resistance to ICIs [5, 6]. The cGAS-STING signaling pathway is a major regulator of innate immune responses and has recently been identified as a critical mediator of endogenous antitumor T cell immunity and response to ICIs [42]. This important role in cancer immune surveillance has motivated the clinical development of cGAMP and other CDN STING agonists as therapeutics to increase tumor immunogenicity [23, 25, 47–50]. Pharmaceutical companies (e.g., Aduro Biotech, Merck, Takeda) have patented synthetic CDNs with improved membrane permeability and/or improved stability relative to cGAMP and other naturally occurring CDNs, and several clinical trials utilizing these molecules are ongoing in the setting of i.t. administration [24, 25]. However, free CDNs have a short systemic circulation half-life and even the more clinically-advanced CDNs still suffer from suboptimal intracellular uptake and bioavailability that strongly limits their drug activity. Nanocarrier systems composed of lipids and polymers have recently been employed for delivery of cGAMP or other CDNs to improve their efficacy as cancer immunotherapeutics. To date, five nanoparticle formulations capable of encapsulating CDNs have been explored for systemic administration, including several variants of liposomal carriers, and STING-NPs, the only polymeric platform described to date for systemic delivery of STING agonists [22, 28–31, 51]. The design of nanocarriers for STING agonists is a nascent area of investigation, and, hence, there exists minimal knowledge of operative drug delivery mechanisms or carrier design criteria for optimizing immunotherapeutic efficacy. Thus, this work provides, to our knowledge, the first comprehensive pharmacological analysis aimed at understanding the fate of an intravenously administered CDN nanocarrier, with potential implications for other nanoscale STING agonists.

A major hurdle for systemic CDN therapy is the short half-life upon intravenous injection that limits delivery to tumors and secondary lymphoid organs. We found that i.v administered cGAMP has a serum half-life of less than 2 mins, which, along with its poor cellular permeability, results in highly inefficient STING pathway activation. The STING-NP platform increases the half-life of cGAMP by ~40-fold and the AUC by 6.5-fold, data similar to that of many nanoparticle drug formulations, which have shown improvements in drug circulation time and exposure [52, 53]. The difference between the pharmacokinetic profile of the polymer and cGAMP may suggest that cGAMP releases from the carrier upon injection, perhaps due to burst release or diffusion across the nanoparticle bilayer under infinite sink conditions [54, 55]. This possibility is supported by data in Figure S6, which demonstrates that cGAMP is completely released from STING-NPs by 4 h and that *in vitro* immunostimulatory activity is reduced in a time-dependent manner following incubation in PBS. Since free cGAMP clears rapidly, it is also probable that cGAMP released from

circulating particles is also cleared quickly, and, therefore, the increase in AUC observed likely reflects the encapsulated drug. Nonetheless, strategies to minimize CDN diffusion or leakage from nanocarriers may further improve pharmacokinetics.

STING-NPs also influence the biodistribution of cGAMP, which, as free drug, minimally accumulated in tissues or tumors due to its short half-life and low AUC. This had a significant impact on cGAMP pharmacodynamics and toxicity. As the largest secondary lymphoid organ with a high density of immune cells, the expression of STING in the spleen is high and, thus, sensitive to activation by cytosolically-delivered cGAMP [37]. Therefore, while the percent injected dose of cGAMP administered with STING-NPs is <2% in the spleen, the relative degree of STING activation is high as reflected by a 50-fold increase in *Ifnb1* expression an hour after administration. This is further supported by studies examining immune cell-level polymer distribution in the spleen where we found that ~40% of macrophages and ~30% of DCs have endocytosed NPs. By contrast, when administered with STING-NPs, ~15% of the injected cGAMP dose accumulates in the liver, which results in a disproportionally mild 10–15-fold increase in *Ifnb1* expression 4–8 h post-administration relative to vehicle controls. This represents approximately the same order of magnitude change in *Ifnb1* expression in the tumor (i.e., 15–20-fold), despite significantly less cGAMP accumulation at tumor sites. While not explicitly demonstrated in our studies, we postulate that Kupffer cells, which have a well-established proclivity for nanoparticle clearance [56], are the primary contributors to STING activation in the liver as previous reports indicate that hepatocytes lack DNA sensing capabilities and have low STING expression [37, 57]. This may allow for hepatic clearance of STING-NPs without significant hepatotoxicity as evidenced by insignificant elevations in ALT and AST following i.v. administration of STING-NPs at the MTD. This may also be reflective of the role of cGAS/STING signaling in Kupffer cells in restraining viral infection, whereas reduced STING levels in hepatocytes have been implicated as a vulnerability to hepatitis B virus infection [58]. Nonetheless, at higher doses of STING-NPs any “buffering capacity” the liver has for STING activation appears to be exceeded, resulting in hepatic necrosis that limits the MTD. Recent work by Sivick *et al.* has demonstrated that high doses of CDN administered locally to tumors is associated with an “ablative” phenotype driven by release of high local levels of proinflammatory cytokines (e.g., TNF-α) that promotes apoptosis of tumor and immune cells [33]. We speculate that a similar response may be manifested in the liver and spleen where the highest levels of STING activation are observed following i.v. STING-NP administration.

STING-NPs, and other nanoparticle-based immunostimulants, have also been shown to transiently increase serum cytokine levels, which may also limit the MTD via several potential mechanisms [59]. It is notable that other systemically administered nanoparticle-based innate immune agonists with a similar cytokine profile to that elicited by STING-NPs have advanced into patients who experienced only transient flu-like symptoms [60]. Moreover, the clinical experience with cancer immunotherapies (e.g., CAR T cells) suggests that some level of systemic cytokine response is well-tolerated and may even be beneficial to outcomes, and strategies are emerging to manage immunotoxicity while maintaining efficacy. Nonetheless, our analysis of the pharmacodynamics and toxicity of STING-NPs at

the MTD implicate the liver and spleen as dose-limiting organs, a finding with important considerations for the further development of STING-activating nanomedicines.

While there is increasing clinical evidence that nanoparticles can preferentially accumulate in human metastatic tumors [61–65], albeit with inter- and intra-patient heterogeneity and via debated mechanisms [61], it is well-established that a relatively low percentage (typically <5%) of injected drug dose reaches the tumor, even in murine models [66, 67]. Consistent with this, we found that ~3% of injected cGAMP reached established (50–100 mm^3) B16-F10 tumors when administered using STING-NPs, which was sufficient to activate the STING pathway as confirmed by western blot and qRT-PCR. Our study also highlights a potentially key distinction between nanoparticle delivery of CDNs and more conventional nanomedicines (e.g., chemotherapy, siRNA) that rely on the delivery of high drug doses to the vast majority of tumor cells at all tumor sites. Our findings, and that of other groups [68, 69], suggest that this may not be as much of a barrier for nanoparticle-based immunostimulants, where passively targeting of a relatively small subset of immune cells can initiate endogenous programs of antitumor immunity that lead to therapeutic responses. Nonetheless, strategies to further improve the delivery of CDNs to tumors must still be explored and driven by a deeper understanding of key cellular targets and optimized STING activation kinetics. For example, chronic STING activation and type I interferon production is associated with autoimmune and chronic inflammatory states [70], and, therefore, prolonged drug accumulation, a goal of many nanomedicines, may not be desirable for CDN delivery. Furthermore, Sivick *et al.* also showed that lower "immunogenic" doses of CDNs can enhance T cell priming and systemic adaptive immunity [33] and, therefore, maximizing STING activation in tumors or lymphoid organs may be counterproductive to optimal immunity. Therefore, whether a slow and sustained or fast "on/off" profile of STING activation is optimal for therapeutic efficacy is still unknown, but should be a consideration for developing the next generation of carriers.

The data provided herein provide the first comprehensive PK-PD analysis of a nanoparticle platform for CDN delivery. Together, the data provide insight into the circulation lifetime of STING-NPs as they distribute, activate the STING pathway, and produce type I interferons and other downstream effectors in tumors as well as major clearance organs. Consequently, using a therapeutic three dose regimen, STING-NPs promoted a cellular remodeling of the tumor immune microenvironment, most notably a >20-fold increase in the number of $CD4^+$ and $CD8^+$ T cells in the tumor. This is consistent with elevated *Cxcl10* in tumors, a key T cell chemokine, and suggests that i.v. administered STING-NPs generate a sufficient chemokine gradient to promote T cell infiltration into established solid tumors, resulting in strong inhibition of tumor growth in B16-F10 and E0771 tumor models as well as modest therapeutic effects in mice bearing YUMM1.7 tumors. While the mechanisms underlying these differences remain to be elucidated, this reduced efficacy may reflect the relatively low tumor mutational load, and therefore antigenicity, of the YUMM1.7 cell line [71], limited tumor distribution or penetration owing to differences in the stromal composition of the TME, and/or differences in the immunocellular composition of the TME that may limit responsiveness to STING agonists. Notably, the ability of i.v. administered STING-NPs to generate a T cell-inflamed TME offers exciting possibilities for developing combination immunoregimens to enhance overall survival. As proof-of-concept, we demonstrated that

i.v. STING-NPs can enhance response to αPD-L1 ICI, which is upregulated in response to STING activation and is therefore a putative resistance mechanism (Figure S7). Intratumorally administered STING agonists have been combined with a number other immunomodulators (e.g., CpG, OX-40, PD-L1), which should also be explored in the context of i.v. STING agonists [72, 73]. Furthermore, the increased tumor infiltration of endogenous T cells observed opens the possibility of using i.v. administered STING-NPs to enhance responses to adoptive T cell transfer or CAR T cell therapy where poor tumor infiltration is a major barrier to efficacy for solid tumors. Future studies will pursue such opportunities.

Conclusion:

Pharmacological activation of the STING pathway is a promising approach for activating anti-tumor innate immunity that results in a remodeling the tumor microenvironment to improve responsiveness to immune checkpoint inhibitors. However, clinical investigation of STING agonists has thus far been limited to i.t. administration to generate abscopal responses, which, while promising, limits clinical utility. Thus, identifying and developing strategies that enable safe and effective systemic administration of STING agonists holds enormous potential for expanding the number of patients that may benefit from this promising therapeutic target. The use of nanoparticle-based drug carriers has recently emerged as a promising approach for enhancing the efficacy of systemically administered CDNs, which suffer from poor drug-like properties and a short i.v. half-life. Using STING-NPs – a polymer-based CDN delivery platform – this work aimed to understand how i.v. administration of CDNs with nanocarriers impacts relationships between pharmacokinetics, pharmacodynamics, toxicity, and therapeutic efficacy. Here, we demonstrate that STING-NPs significantly extend the elimination half-life of cGAMP by 40-fold, resulting in a modest, but significant, increase in tumor accumulation of cGAMP with an attendant increase in STING activation in the TME. This also changed the biodistribution profile of cGAMP, resulting in increased STING activation in the spleen and liver, which restricted the MTD. Nonetheless, i.v. administration of STING-NPs dramatically increased the number of tumor-infiltrating T cells in poorly immunogenic B16-F10 tumors, resulting in enhanced therapeutic efficacy, a result validated in additional syngeneic murine tumor models. Together, these data, which represent the first rigorous investigation into the PK-PD relationship of a STING-activating nanomedicine, demonstrate that STING-NPs open a therapeutic window for systemic administration of CDNs and provide new insight into operative design criteria for engineering of optimized delivery platforms for systemic delivery of STING agonists.

Supplementary Material

Refer to Web version on PubMed Central for supplementary material.

Acknowledgements:

The authors would like to thank Dr. Marcus Bosenberg for the generous donation YUMM1.7 cells, Dr. Craig Duvall for use of IVIS Imaging System, and the Vanderbilt Brain Institute for use of the scintillation counter. We thank the core facilities of the Vanderbilt Institute of Nanoscale Sciences and Engineering (VINSE), the

VUMC Flow Cytometry Shared Resource, supported by the Vanderbilt Ingram Cancer Center (P30 CA68485) and the Vanderbilt Digestive Disease Research Center (DK058404), and Vanderbilt Translational Pathology Shared Resource (supported in part by the NCI/NIH Cancer Center Support Grant 5P30 CA684850-19). 2'3'-cGAMP was provided by the Vanderbilt Institute of Chemical Biology Chemical Synthesis Core. This research was supported by grants from the National Science Foundation CBET-1554623 (JTW), a Vanderbilt Ingram Cancer Center (VICC) Ambassador Discovery Grant (JTW), the Melanoma Research Alliance 503565 (JTW), Susan G. Komen CCR19609205 (JTW), Department of Defense Era of Hope Scholar Award BC170037 (JMB), the National Institutes of Health R01 CA245134 (JTW), and also supported by a Stand Up To Cancer Innovative Research Grant, Grant Number SU2C-AACR-IRG 20-17 (JTW). Stand Up To Cancer (SU2C) is a program of the Entertainment Industry Foundation. Research grants are administered by the American Association for Cancer Research, the scientific partner of SU2C. MW acknowledges postdoctoral funding support from the Canadian Institute of Health Research (CIHR). Graphical abstract image made with BioRender.com.

References:

[1]. Hastings MPR, Karen T, Immune Checkpoint Inhibitors in the Treatment of Melanoma: From Basic Science to Clinical Application, (2017).

[2]. Ribas A, Wolchok JD, Cancer immunotherapy using checkpoint blockade, Science, 359 (2018) 1350–1355. [PubMed: 29567705]

[3]. Sharma P, Allison JP, The future of immune checkpoint therapy, Science, 348 (2015) 56–61. [PubMed: 25838373]

[4]. Ugurel S, Rohmel J, Ascierto PA, Flaherty KT, Grob JJ, Hauschild A, Larkin J, Long GV, Lorigan P, McArthur GA, Ribas A, Robert C, Schadendorf D, Garbe C, Survival of patients with advanced metastatic melanoma: the impact of novel therapies-update 2017, Eur J Cancer, 83 (2017) 247–257. [PubMed: 28756137]

[5]. Binnewies M, Roberts EW, Kersten K, Chan V, Fearon DF, Merad M, Coussens LM, Gabrilovich DI, Ostrand-Rosenberg S, Hedrick CC, Vonderheide RH, Pittet MJ, Jain RK, Zou W, Howcroft TK, Woodhouse EC, Weinberg RA, Krummel MF, Understanding the tumor immune microenvironment (TIME) for effective therapy, Nat Med, 24 (2018) 541–550. [PubMed: 29686425]

[6]. Chen DS, Mellman I, Elements of cancer immunity and the cancer-immune set point, Nature, 541 (2017) 321–330. [PubMed: 28102259]

[7]. Hegde PS, Karanikas V, Evers S, The Where, the When, and the How of Immune Monitoring for Cancer Immunotherapies in the Era of Checkpoint Inhibition, Clin Cancer Res, 22 (2016) 1865–1874. [PubMed: 27084740]

[8]. Hanahan D, Weinberg RA, Hallmarks of cancer: the next generation, Cell, 144 (2011) 646–674. [PubMed: 21376230]

[9]. Galon J, Bruni D, Approaches to treat immune hot, altered and cold tumours with combination immunotherapies, Nat Rev Drug Discov, 18 (2019) 197–218. [PubMed: 30610226]

[10]. Bonaventura P, Shekarian T, Alcazer V, Valladeau-Guilemond J, Valsesia-Wittmann S, Amigorena S, Caux C, Depil S, Cold Tumors: A Therapeutic Challenge for Immunotherapy, Front Immunol, 10 (2019).

[11]. Shekarian T, Valsesia-Wittmann S, Brody J, Michallet MC, Depil S, Caux C, Marabelle A, Pattern recognition receptors: immune targets to enhance cancer immunotherapy, Ann Oncol, 28 (2017) 1756–1766. [PubMed: 28444111]

[12]. Liu Z, Han C, Fu YX, Targeting innate sensing in the tumor microenvironment to improve immunotherapy, Cell Mol Immunol, 17 (2020) 13–26. [PubMed: 31844141]

[13]. Koster BD, van den Hout M, Sluijter BJR, Molenkamp BG, Vuylsteke R, Baars A, van Leeuwen PAM, Scheper RJ, Petrousjka M. van den Tol, van den Eertwegh AJM, de Gruijl TD, Local Adjuvant Treatment with Low-Dose CpG-B Offers Durable Protection against Disease Recurrence in Clinical Stage I-II Melanoma: Data from Two Randomized Phase II Trials, Clin Cancer Res, 23 (2017) 5679–5686. [PubMed: 28972083]

[14]. Hammerich L, Marron TU, Upadhyay R, Svensson-Arvelund J, Dhainaut M, Hussein S, Zhan Y, Ostrowski D, Yellin M, Marsh H, Salazar AM, Rahman AH, Brown BD, Merad M, Brody JD, Systemic clinical tumor regressions and potentiation of PD1 blockade with in situ vaccination, Nat Med, 25 (2019) 814–824. [PubMed: 30962585]

[15]. Yang H, Lee WS, Kong SJ, Kim CG, Kim JH, Chang SK, Kim S, Kim G, Chon HJ, Kim C, STING activation reprograms tumor vasculatures and synergizes with VEGFR2 blockade, J Clin Invest, 130 (2019) 4350–4364.

[16]. Ager CR, Reilley MJ, Nicholas C, Bartkowiak T, Jaiswal AR, Curran MA, Intratumoral STING activation with T-cell checkpoint modulation generates systemic antitumor immunity, Cancer Immunol Res, 5 (2017) 676–684. [PubMed: 28674082]

[17]. Wang-Bishop L, Wehbe M, Shae D, James J, Hacker BC, Garland K, Chistov PP, Rafat M, Balko JM, Wilson JT, Potent STING activation stimulates immunogenic cell death to enhance antitumor immunity in neuroblastoma, in: J Immunother Cancer, 2020.

[18]. Dubensky TW Jr., Kanne DB, Leong ML, Rationale, progress and development of vaccines utilizing STING-activating cyclic dinucleotide adjuvants, Ther Adv Vaccines, 1 (2013) 131–143. [PubMed: 24757520]

[19]. Lioux T, Mauny MA, Lamoureux A, Bascoul N, Hays M, Vernejoul F, Baudru AS, Boularan C, Lopes-Vicente J, Qushair G, Tiraby G, Design, Synthesis, and Biological Evaluation of Novel Cyclic Adenosine-Inosine Monophosphate (cAIMP) Analogs That Activate Stimulator of Interferon Genes (STING), J Med Chem, 59 (2016) 10253–10267. [PubMed: 27783523]

[20]. Li L, Yin Q, Kuss P, Maliga Z, Millan JL, Wu H, Mitchison TJ, Hydrolysis of 2'3'-cGAMP by ENPP1 and design of nonhydrolyzable analogs, Nat Chem Biol, 10 (2014) 1043–1048. [PubMed: 25344812]

[21]. Ager CR, Reilley MJ, Nicholas C, Bartkowiak T, Jaiswal AR, Curran MA, Intratumoral STING Activation with T-cell Checkpoint Modulation Generates Systemic Antitumor Immunity, Cancer Immunol Res, 5 (2017) 676–684. [PubMed: 28674082]

[22]. Koshy ST, Cheung AS, Gu L, Graveline AR, Mooney DJ, Liposomal Delivery Enhances Immune Activation by STING Agonists for Cancer Immunotherapy, Adv Biosyst, 1 (2017).

[23]. Corrales L, Glickman LH, McWhirter SM, Kanne DB, Sivick KE, Katibah GE, Woo SR, Lemmens E, Banda T, Leong JJ, Metchette K, Dubensky TW Jr., Gajewski TF, Direct Activation of STING in the Tumor Microenvironment Leads to Potent and Systemic Tumor Regression and Immunity, Cell Rep, 11 (2015) 1018–1030. [PubMed: 25959818]

[24]. Mullard A, Can innate immune system targets turn up the heat on 'cold' tumours?, in: Nat Rev Drug Discov, England, 2018, pp. 3–5.

[25]. Flood BA, Higgs EF, Li S, Luke JJ, Gajewski TF, STING pathway agonism as a cancer therapeutic, Immunol Rev, 290 (2019) 24–38. [PubMed: 31355488]

[26]. Irvine DJ, Dane EL, Enhancing cancer immunotherapy with nanomedicine, Nat Rev Immunol, (2020).

[27]. Marabelle A, Kohrt H, Caux C, Levy R, Intratumoral immunization: a new paradigm for cancer therapy., Clinical cancer research : an official journal of the American Association for Cancer Research, 20 (2014) 1747–1756. [PubMed: 24691639]

[28]. Cheng N, Watkins-Schulz R, Junkins RD, David CN, Johnson BM, Montgomery SA, Peine KJ, Darr DB, Yuan H, McKinnon KP, Liu Q, Miao L, Huang L, Bachelder EM, Ainslie KM, Ting JP, A nanoparticle-incorporated STING activator enhances antitumor immunity in PD-L1-insensitive models of triple-negative breast cancer, JCI Insight, 3 (2018).

[29]. Nakamura T, Miyabe H, Hyodo M, Sato Y, Hayakawa Y, Harashima H, Liposomes loaded with a STING pathway ligand, cyclic di-GMP, enhance cancer immunotherapy against metastatic melanoma, J Control Release, 216 (2015) 149–157. [PubMed: 26282097]

[30]. Miyabe H, Hyodo M, Nakamura T, Sato Y, Hayakawa Y, Harashima H, A new adjuvant delivery system 'cyclic di-GMP/YSK05 liposome' for cancer immunotherapy, J Control Release, 184 (2014) 20–27. [PubMed: 24727060]

[31]. Shae D, Becker KW, Christov P, Yun DS, Lytton-Jean AKR, Sevimli S, Ascano M, Kelley M, Johnson DB, Balko JM, Wilson JT, Endosomolytic polymersomes increase the activity of cyclic dinucleotide STING agonists to enhance cancer immunotherapy, Nat Nanotechnol, 14 (2019) 269–278. [PubMed: 30664751]

[32]. Wang-Bishop L, Wehbe M, Shae D, James J, Hacker BC, Garland K, Chistov PP, Rafat M, Balko JM, Wilson JT, Potent STING activation stimulates immunogenic cell death to enhance antitumor immunity in neuroblastoma, J Immunother Cancer, 8 (2020).

[33]. Sivick KE, Desbien AL, Glickman LH, Reiner GL, Corrales L, Surh NH, Hudson TE, Vu UT, Francica BJ, Banda T, Katibah GE, Kanne DB, Leong JJ, Metchette K, Bruml JR, Ndubaku CO, McKenna JM, Feng Y, Zheng L, Bender SL, Cho CY, Leong ML, van Elsas A, Dubensky TW Jr., McWhirter SM, Magnitude of Therapeutic STING Activation Determines CD8(+) T Cell-Mediated Anti-tumor Immunity, Cell Rep, 25 (2018) 3074–3085.e3075.

[34]. NCBI-GENE, STING1 stimulator of interferon response cGAMP interactor 1 [Homo sapiens (human)] - Gene - NCBI, in, Pubs, 2020.

[35]. Lewis SM, Williams A, Eisenbarth SC, Structure-function of the immune system in the spleen, Sci Immunol, 4 (2019).

[36]. Gulen MF, Koch U, Haag SM, Schuler F, Apetoh L, Villunger A, Radtke F, Ablasser A, Signalling strength determines proapoptotic functions of STING, Nat Commun, 8 (2017) 427. [PubMed: 28874664]

[37]. Thomsen MK, Nandakumar R, Stadler D, Malo A, Valls RM, Wang F, Reinert LS, Dagnaes-Hansen F, Hollensen AK, Mikkelsen JG, Protzer U, Paludan SR, Lack of immunological DNA sensing in hepatocytes facilitates hepatitis B virus infection, Hepatology, 64 (2016) 746–759. [PubMed: 27312012]

[38]. Xu H, Paxton J, Lim J, Li Y, Zhang W, Duxfield L, Wu Z, Development of high-content gemcitabine PEGylated liposomes and their cytotoxicity on drug-resistant pancreatic tumour cells, Pharm Res, 31 (2014) 2583–2592. [PubMed: 24639234]

[39]. Yoshizawa Y, Kono Y, Ogawara K, Kimura T, Higaki K, PEG liposomalization of paclitaxel improved its in vivo disposition and anti-tumor efficacy, Int J Pharm, 412 (2011) 132–141. [PubMed: 21507344]

[40]. Huang W, Zhang J, Dorn HC, Zhang C, Assembly of bio-nanoparticles for double controlled drug release, PLoS One, 8 (2013) e74679.

[41]. Lu XY, Wu DC, Li ZJ, Chen GQ, Polymer nanoparticles, Prog Mol Biol Transl Sci, 104 (2011) 299–323. [PubMed: 22093222]

[42]. Zhu Y, An X, Zhang X, Qiao Y, Zheng T, Li X, STING: a master regulator in the cancer-immunity cycle, in: Mol Cancer, 2019.

[43]. Munn DH, Mellor AL, The tumor-draining lymph node as an immune-privileged site, Immunol Rev, 213 (2006) 146–158. [PubMed: 16972902]

[44]. Dai Q, Wilhelm S, Ding D, Syed AM, Sindhwani S, Zhang Y, Chen YY, MacMillan P, Chan WCW, Quantifying the Ligand-Coated Nanoparticle Delivery to Cancer Cells in Solid Tumors, ACS Nano, 12 (2018) 8423–8435. [PubMed: 30016073]

[45]. Kourtis IC, Hirosue S, de Titta A, Kontos S, Stegmann T, Hubbell JA, Swartz MA, Peripherally administered nanoparticles target monocytic myeloid cells, secondary lymphoid organs and tumors in mice, PLoS One, 8 (2013) e61646.

[46]. Bronte V, Pittet MJ, The spleen in local and systemic regulation of immunity, Immunity, 39 (2013) 806–818. [PubMed: 24238338]

[47]. Demaria O, Gassart AD, Coso S, Gestermann N, Domizio JD, Flatz L, Gaide O, Michielin O, Hwu P, Petrova TV, Martinon F, Modlin RL, Speiser DE, Gilliet M, STING activation of tumor endothelial cells initiates spontaneous and therapeutic antitumor immunity, PNAS, 112 (2015) 15408–15413. [PubMed: 26607445]

[48]. Ohkuri T, Kosaka A, Ishibashi K, Kumai T, Hirata Y, Ohara K, Nagato T, Oikawa K, Aoki N, Harabuchi Y, Celis E, Kobayashi H, Intratumoral administration of cGAMP transiently accumulates potent macrophages for anti-tumor immunity at a mouse tumor site, Cancer Immunol Immunother, 66 (2017) 705–716. [PubMed: 28243692]

[49]. Curran E, Chen X, Corrales L, Kline DE, Dubensky TW Jr., Duttagupta P, Kortylewski M, Kline J, STING Pathway Activation Stimulates Potent Immunity against Acute Myeloid Leukemia, Cell Rep, 15 (2016) 2357–2366. [PubMed: 27264175]

[50]. Fu J, Kanne DB, Leong M, Glickman LH, McWhirter SM, Lemmens E, Mechette K, Leong JJ, Lauer P, Liu W, Sivick KE, Zeng Q, Soares KC, Zheng L, Portnoy DA, Woodward JJ, Pardoll DM, Dubensky TW Jr., Kim Y, STING agonist formulated cancer vaccines can cure established tumors resistant to PD-1 blockade, Sci Transl Med, 7 (2015) 283ra252.

[51]. Atukorale PU, Raghunathan SP, Raguveer V, Moon TJ, Zheng C, Bielecki PA, Wiese ML, Goldberg AL, Covarrubias G, Hoimes CJ, Karathanasis E, Nanoparticle Encapsulation of Synergistic Immune Agonists Enables Systemic Codelivery to Tumor Sites and IFNbeta-Driven Antitumor Immunity, Cancer Res, 79 (2019) 5394–5406. [PubMed: 31431457]

[52]. Tucci ST, Kheirolomoom A, Ingham ES, Mahakian LM, Tam SM, Foiret J, Hubbard NE, Borowsky AD, Baikoghli M, Cheng RH, Ferrara KW, Tumor-specific delivery of gemcitabine with activatable liposomes, J Control Release, 309 (2019) 277–288. [PubMed: 31301340]

[53]. Udofot O, Affram K, Smith T, Tshabe B, Krishnan S, Sachdeva M, Agyare E, Pharmacokinetic, biodistribution and therapeutic efficacy of 5-fluorouracil-loaded pH-sensitive PEGylated liposomal nanoparticles in HCT-116 tumor bearing mouse, J Nat Sci, 2 (2016).

[54]. Thomas AM, Kapanen AI, Hare JI, Ramsay E, Edwards K, Karlsson G, Bally MB, Development of a liposomal nanoparticle formulation of 5-fluorouracil for parenteral administration: formulation design, pharmacokinetics and efficacy, J Control Release, 150 (2011) 212–219. [PubMed: 21094191]

[55]. Wehbe M, Anantha M, Shi M, Leung A, Dragowska WH, Sanche L, Bally MB, Development and optimization of an injectable formulation of copper diethyldithiocarbamate, an active anticancer agent, in: Int J Nanomedicine, 2017, pp. 4129–4146. [PubMed: 28615941]

[56]. Tsoi KM, MacParland SA, Ma XZ, Spetzler VN, Echeverri J, Ouyang B, Fadel SM, Sykes EA, Goldaracena N, Kaths JM, Conneely JB, Alman BA, Selzner M, Ostrowski MA, Adeyi OA, Zilman A, McGilvray ID, Chan WC, Mechanism of hard nanomaterial clearance by the liver, Nat Mater, 15 (2016) 1212–1221. [PubMed: 27525571]

[57]. Lei Z, Deng M, Yi Z, Sun Q, Shapiro RA, Xu H, Li T, Loughran PA, Griepentrog JE, Huang H, Scott MJ, Huang F, Billiar TR, cGAS-mediated autophagy protects the liver from ischemia-reperfusion injury independently of STING, in: Am J Physiol Gastrointest Liver Physiol, 2018, pp. G655–667. [PubMed: 29446653]

[58]. Cheng X, Xia Y, Serti E, Block PD, Chung M, Chayama K, Rehermann B, Liang TJ, Hepatitis B virus evades innate immunity of hepatocytes but activates macrophages during infection, Hepatology, 66 (2017) 1779–1793. [PubMed: 28665004]

[59]. Tisoncik JR, Korth MJ, Simmons CP, Farrar J, Martin TR, Katze MG, Into the Eye of the Cytokine Storm, in: Microbiol Mol Biol Rev, 2012, pp. 16–32. [PubMed: 22390970]

[60]. Kranz LM, Diken M, Haas H, Kreiter S, Loquai C, Reuter KC, Meng M, Fritz D, Vascotto F, Hefesha H, Grunwitz C, Vormehr M, Husemann Y, Selmi A, Kuhn AN, Buck J, Derhovanessian E, Rae R, Attig S, Diekmann J, Jabulowsky RA, Heesch S, Hassel J, Langguth P, Grabbe S, Huber C, Tureci O, Sahin U, Systemic RNA delivery to dendritic cells exploits antiviral defence for cancer immunotherapy, Nature, 534 (2016) 396–401. [PubMed: 27281205]

[61]. Man F, Lammers T, R T.M.d.R., Imaging Nanomedicine-Based Drug Delivery: a Review of Clinical Studies, Mol Imaging Biol, 20 (2018) 683–695. [PubMed: 30084044]

[62]. Rastinehad AR, Anastos H, Wajswol E, Winoker JS, Sfakianos JP, Doppalapudi SK, Carrick MR, Knauer CJ, Taouli B, Lewis SC, Tewari AK, Schwartz JA, Canfield SE, George AK, West JL, Halas NJ, Gold nanoshell-localized photothermal ablation of prostate tumors in a clinical pilot device study, Proc Natl Acad Sci U S A, 116 (2019) 18590–18596. [PubMed: 31451630]

[63]. Lee H, Shields AF, Siegel BA, Miller KD, Krop I, Ma CX, LoRusso PM, Munster PN, Campbell K, Gaddy DF, Leonard SC, Geretti E, Blocker SJ, Kirpotin DB, Moyo V, Wickham TJ, Hendriks BS, (64)Cu-MM-302 Positron Emission Tomography Quantifies Variability of Enhanced Permeability and Retention of Nanoparticles in Relation to Treatment Response in Patients with Metastatic Breast Cancer, Clin Cancer Res, 23 (2017) 4190–4202. [PubMed: 28298546]

[64]. Ramanathan RK, Korn RL, Raghunand N, Sachdev JC, Newbold RG, Jameson G, Fetterly GJ, Prey J, Klinz SG, Kim J, Cain J, Hendriks BS, Drummond DC, Bayever E, Fitzgerald JB, Correlation between Ferumoxytol Uptake in Tumor Lesions by MRI and Response to Nanoliposomal Irinotecan in Patients with Advanced Solid Tumors: A Pilot Study, Clin Cancer Res, 23 (2017) 3638–3648. [PubMed: 28159813]

[65]. Harrington KJ, Mohammadtaghi S, Uster PS, Glass D, Peters AM, Vile RG, Stewart JS, Effective targeting of solid tumors in patients with locally advanced cancers by radiolabeled pegylated liposomes, Clin Cancer Res, 7 (2001) 243–254. [PubMed: 11234875]

[66]. Shao K, Singha S, Clemente-Casares X, Tsai S, Yang Y, Santamaria P, Nanoparticle-based immunotherapy for cancer, ACS Nano, 9 (2015) 16–30. [PubMed: 25469470]

[67]. Das M, Shen L, Liu Q, Goodwin TJ, Huang L, Nanoparticle Delivery of RIG-I Agonist Enables Effective and Safe Adjuvant Therapy in Pancreatic Cancer, Mol Ther, 27 (2019) 507–517. [PubMed: 30545600]

[68]. Jiang W, Yuan H, Chan CK, von Roemeling CA, Yan Z, Weissman IL, Kim BYS, Lessons from immuno-oncology: a new era for cancer nanomedicine?, Nat Rev Drug Discov, 16 (2017) 369–370. [PubMed: 28303024]

[69]. Wilhelm S, Tavares AJ, Dai Q, Ohta S, Audet J, Dvorak HF, Chan WCW, Analysis of nanoparticle delivery to tumours, Nature Reviews Materials, 1 (2016) 16014.

[70]. Barber GN, STING: infection, inflammation and cancer, in: Nat Rev Immunol, 2015, pp. 760–770. [PubMed: 26603901]

[71]. Wang J, Perry CJ, Meeth K, Thakral D, Damsky W, Micevic G, Kaech S, Blenman K, Bosenberg M, UV-induced somatic mutations elicit a functional T cell response in the YUMMER1.7 mouse melanoma model, Pigment cell & melanoma research, 30 (2017) 428–435. [PubMed: 28379630]

[72]. Temizoz B, Kuroda E, Ohata K, Jounai N, Ozasa K, Kobiyama K, Aoshi T, Ishii KJ, TLR9 and STING agonists synergistically induce innate and adaptive type-II IFN, Eur J Immunol, 45 (2015) 1159–1169. [PubMed: 25529558]

[73]. Foote JB, Kok M, Leatherman JM, Armstrong TD, Marcinkowski BC, Ojalvo LS, Kanne DB, Jaffee EM, Dubensky TW, Emens LA, A STING agonist given with OX40 receptor and PD-L1 modulators primes immunity and reduces tumor growth in tolerized mice, Cancer Immunol Res, 5 (2017) 468–479. [PubMed: 28483787]

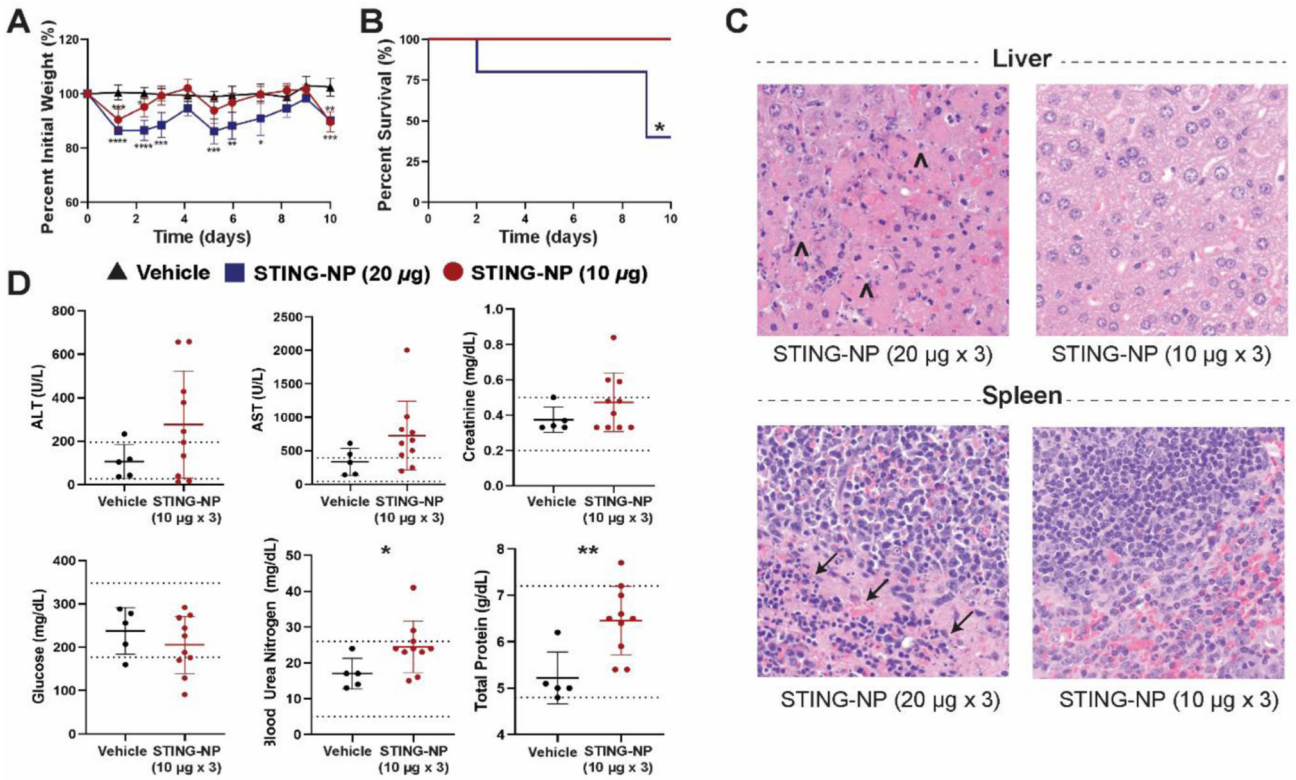

Figure 1: Determination of maximum tolerated dose for STING-NP.

C57BL/6 mice were treated with Vehicle or STING-NPs at 10 or 20 µg per mouse intravenously every 3 days for a total of 3 injections. Mice were weighed and monitored for 10 days; the percent initial body weight **(A)** and survival **(B)** were plotted. On day 10, mice were euthanized and the organs were formalin fixed for gross pathology. **(C)** H&E staining of liver and spleen images showing necrosis (Λ) in the liver and apoptosis (→) in the spleen. **(D)** Blood chemistry of mice treated with STING-NPs at 24 hours after final injection. **P*<0.05, ** *P*<0.01, *** *P*<0.001, **** *P*<0.0001, indicate a statistically significant difference relative to vehicle (PBS).

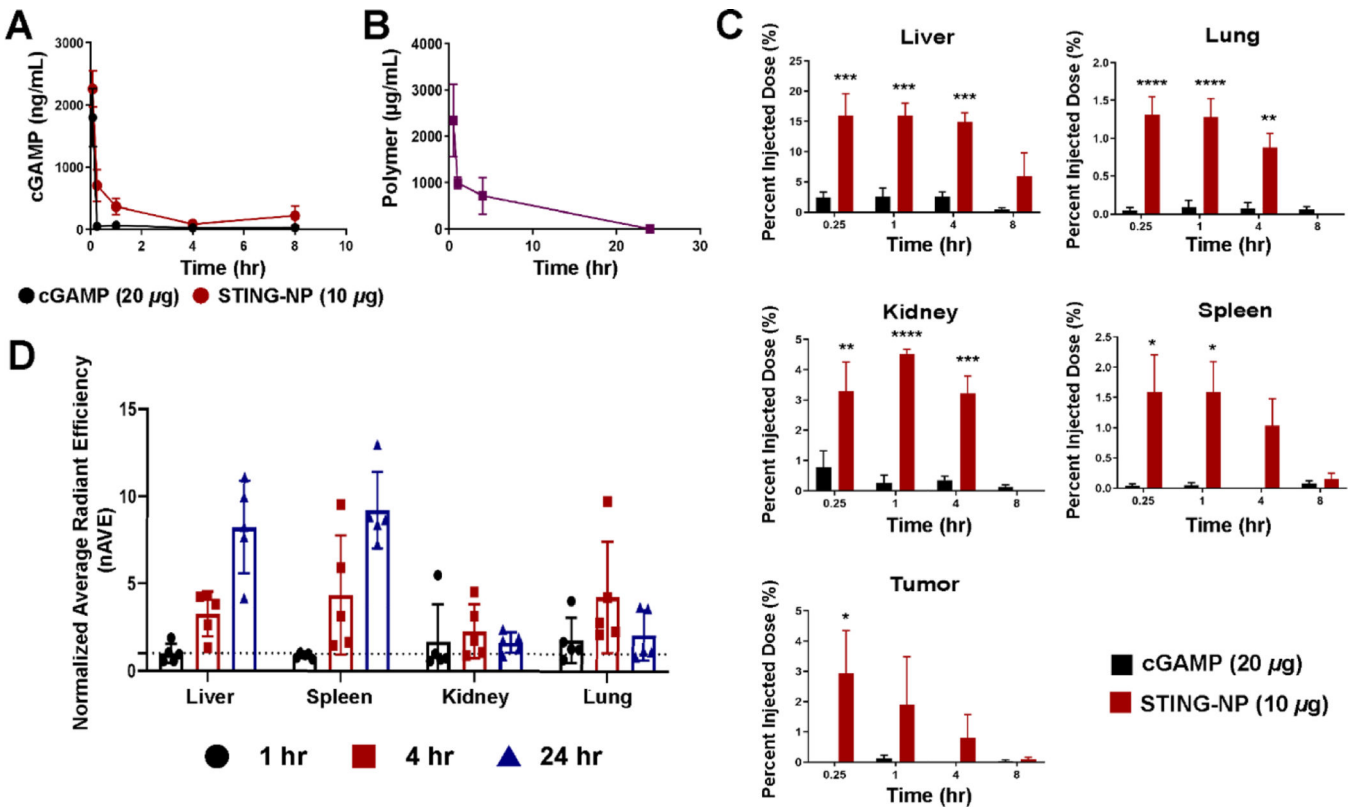

Figure 2: STING-NPs improve cGAMP pharmacokinetics and alter thebiodistribution profile.

6–8-week-old C57BL/6 mice were inoculated with B16-F10 tumor cells. When tumors reached 100–200 mm^3, mice were treated with cGAMP (1 μCi per mouse, 20 μg of cGAMP) or STING-NP (1 μCi per mouse, 10 μg cGAMP) and euthanized at indicated timepoints. (**A**) Plasma cGAMP concentrations as a function of time obtained through scintillation counting. (**B**) Plasma polymer concentration as a function of time measured through fluorescence of Cy5-labelled polymer spiked at a 1:5 ratio used to make polymersomes. (**C**) Organ cGAMP distribution as a function of time plotted as percent injected dose. (**D**) Organ polymer distribution using IVIS imagine at indicated time points from whole organs. Data were normalized to vehicle treated organs. *P<0.05, ** P<0.01, *** P<0.001, **** P<0.0001 indicate a statistically significant difference relative to cGAMP. n=4–5 mice per group with data plotted as mean ± SEM.

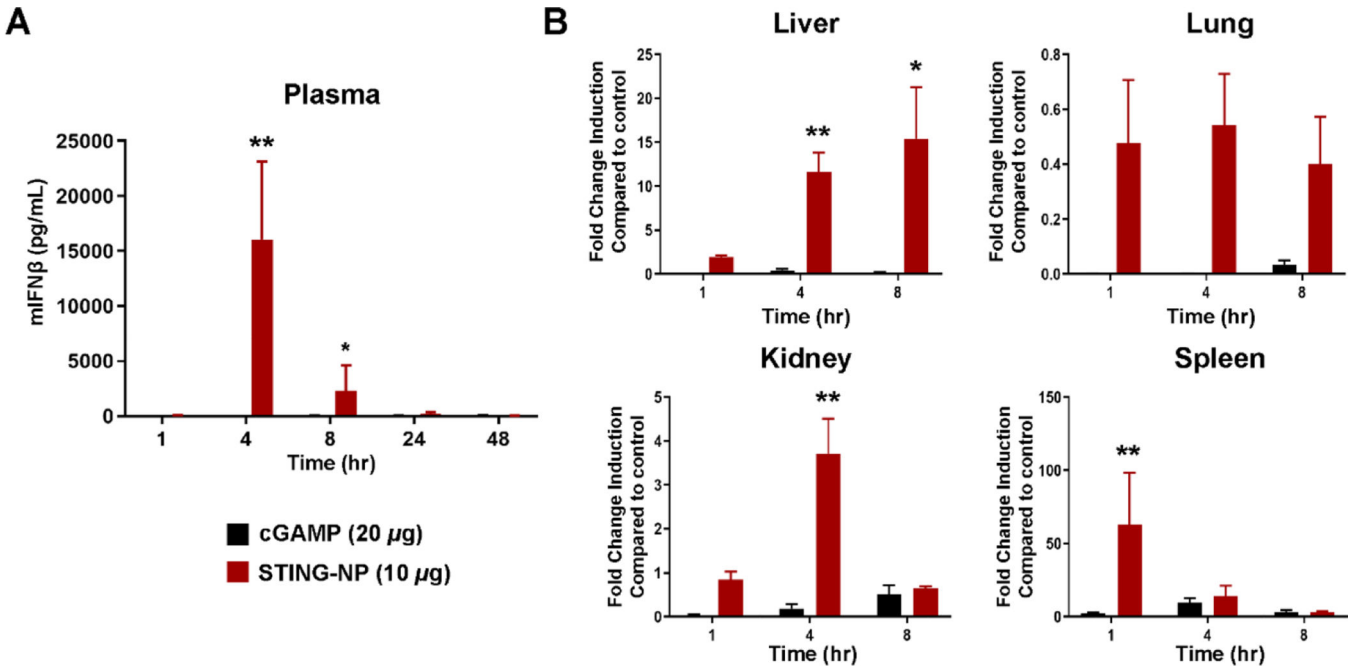

Figure 3: STING-NPs activate a type-I interferon response in blood and clearance organs.

6–8-week-old C57BL/6 mice were treated with vehicle, cGAMP (20 μg per mouse) or STING-NP (10 μg cGAMP per mouse) and euthanized at indicated timepoints. (**A**) Plasma mouse interferon beta was measured by ELISA. (**B**) qRT-PCR was used to measure *Ifnb1* transcript levels in liver, lung, kidney, and spleens. Data are plotted as fold change over vehicle treated mice. **P*<0.05, ** *P*<0.01, *** *P*<0.001, **** *P*<0.0001 indicate a statistically significant difference relative to cGAMP. n=4 mice per group with data plotted as mean ± SEM, qPCR data are shown as fold change over vehicle treated mice.

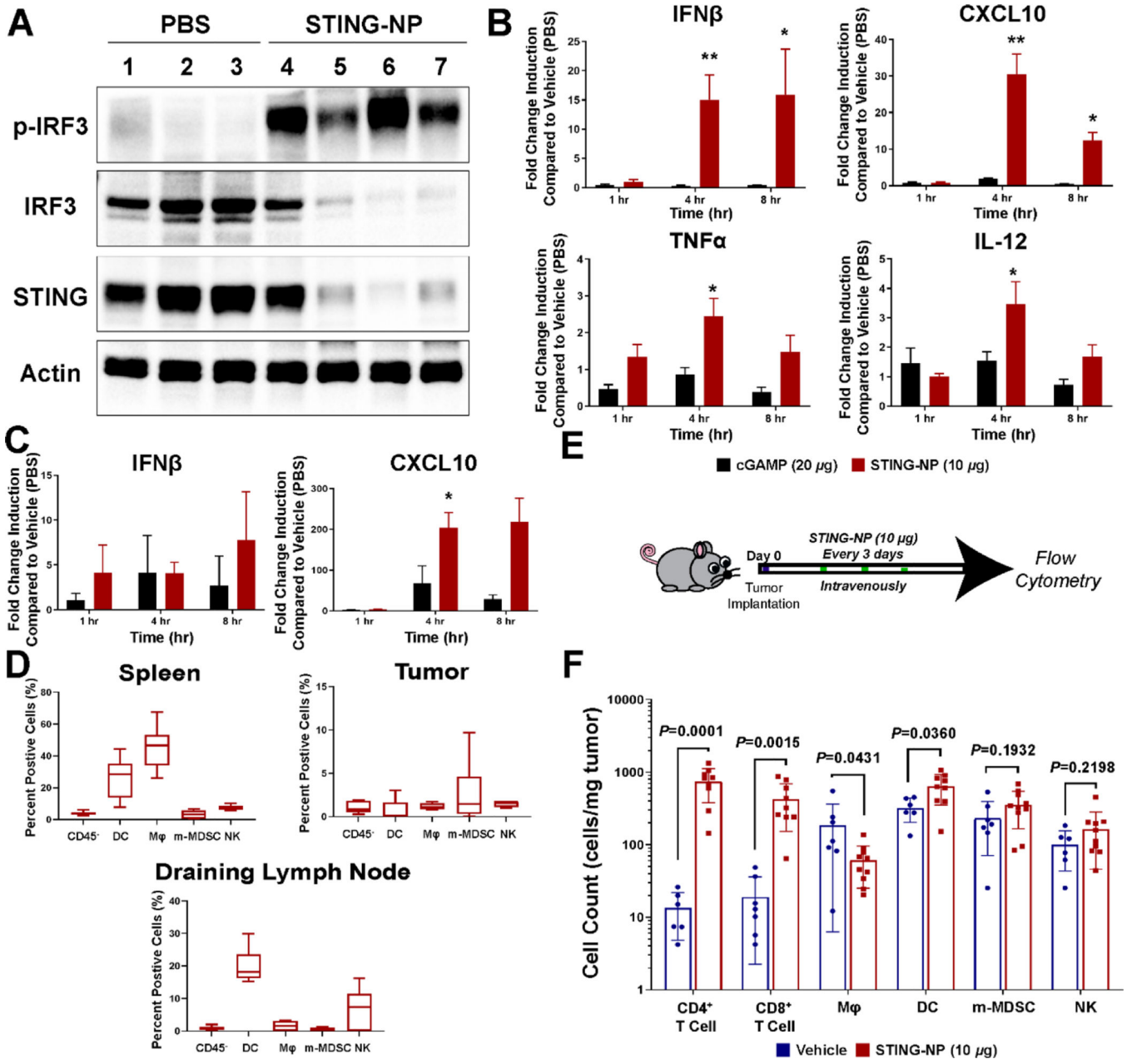

Figure 4: Systemic STING-NP treatment causes STING activation in tumors and remodeling of the TME.

(**A**) 6–8-week-old C57BL/6 B16-F10 tumor bearing mice were treated with vehicle or STING-NP (10 μg cGAMP per mouse). Western blot analysis of tumors 24 hours after treatment examining STING and IRF3/p-IRF3 expression. (**B**) qRT-PCR was used to measure *Ifnb1*, *Cxcl10*, *Tnfa*, and *Il12* transcript levels in Vehicle (PBS), cGAMP or STING-NP treated tumor, data is shown as fold change over vehicle. (**C**) qRT-PCR was used to measure lymph node *Ifnb1* and *Cxcl10* transcript levels in Vehicle (PBS), cGAMP or STING-NP treated lymph node, data is shown as fold change over vehicle. (**D**) Mice were treated with Cy5-labelled polymersomes and euthanized at 24 h post-injection. Data are plotted as percentage of Cy5-positive cells in spleen, tumor, and draining lymph node.

(**E**) Mouse treatment scheme for flow cytometry study, 100 mm^3 tumors were treated thrice and harvest 24 hrs after final injection for characterization. (**F**) Immune cell infiltration into B16-F10 tumors obtained 24 hours after third vehicle/STING-NP treatment analyzed using flow cytometry. *P<0.05, **P<0.01, ***P<0.001, ****P<0.0001 indicate a statistically significant difference relative to cGAMP (B/E) or vehicle (D). Data shown as mean ± SEM (qPCR is fold change as compared to vehicle treated tumors/lymph node, n=4) and mean ± SD (flow cytometry, n= 6–10).

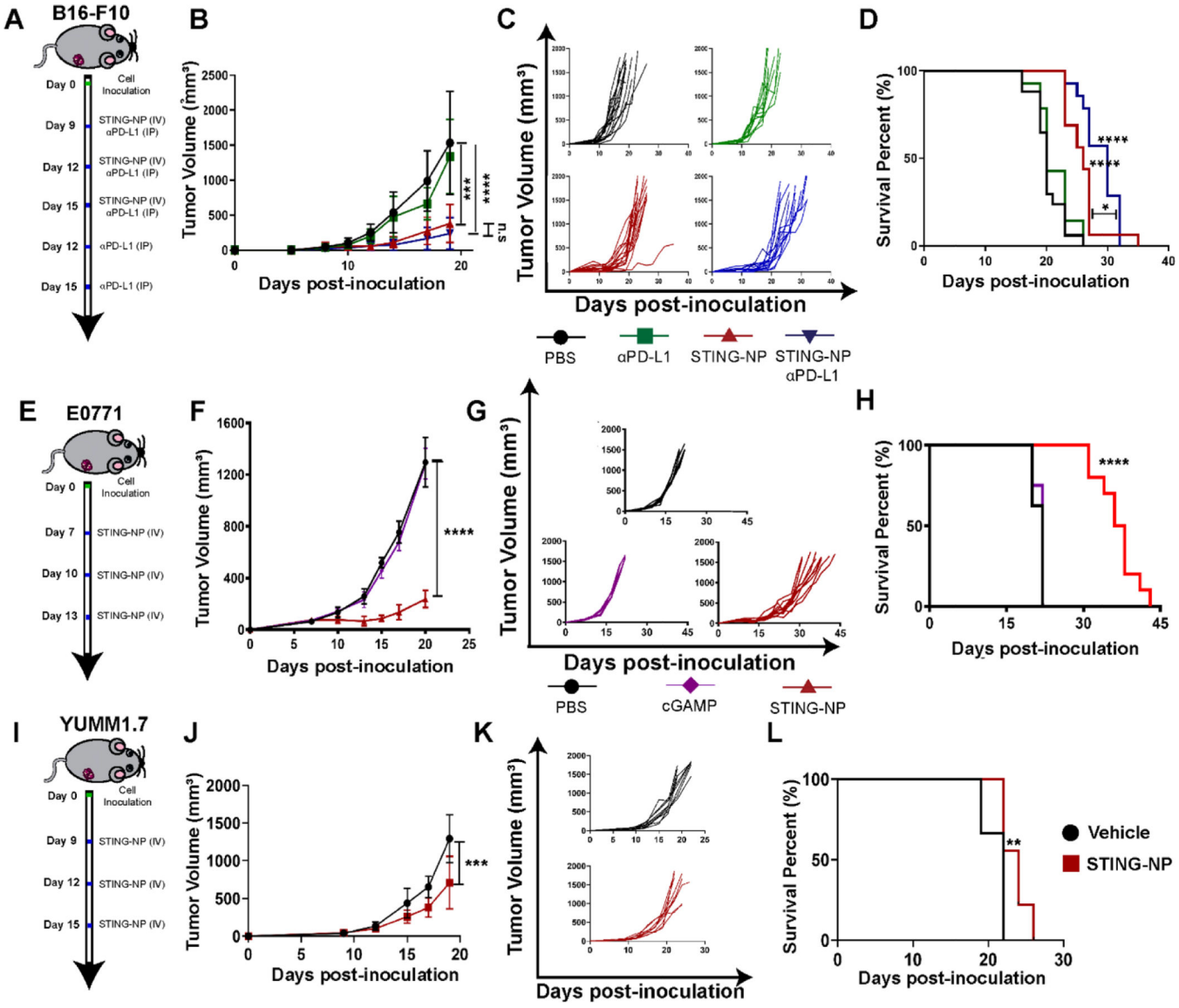

Figure 5: STING-NP efficacy in melanoma and breast cancer models.

(**A**) Schematic summary of treatment for mice with B16-F10 tumors. (**B**) Average tumor volume and (**C**) spider plots for treated and untreated tumors. (**D**) Kaplan-Meier survival curves of mice treated with indicated formulation. (E) Schematic representation of study design and treatment regimen for E0771 breast cancer model. (**F**) Average tumor volume, (**G**) spider plots, and (**H**) Kaplan-Meier survival curves for mice injected intravenously with vehicle or STING-NP. (I) Schematic representation of study design and treatment regimen for YUMM1.7 tumor model. (**J**) Average tumor volume, (**K**) spider plots, and (**L**) Kaplan-Meier survival curves for mice injected intravenously with vehicle or STING-NP. Mice were treated with indicated formulation using a total tumor volume >1500 mm^3 as endpoint criteria.* $P<0.05$, ** $P<0.01$, *** $P<0.001$, **** $P<0.0001$ indicate a statistically significant difference relative to vehicle (PBS). Data plotted as mean ± SD, n= 6–10 mice per group. B16-F10 and E0771 tumor volumes were compared on day 19 using a one-way ANOVA

using Tukey's post-hoc test. YUMM1.7 tumor volumes were compared by Student's t-test. Kaplan–Meier survival analysis (two-tailed Mantel–Cox test).

Table 1:

Pharmacokinetic parameters for cGAMP and STING-NP

Treatment	cGAMP Half-life (hr)	cGAMP $AUC_{0\text{-}inf}$ (μg•hr/mL)	Polymer Half-life (hr)	Polymer $AUC_{0\text{-}inf}$ (μg•hr/mL)
Free cGAMP	0.033	851.3	-	-
STING-NP	1.3	5564.4	6.4	11453.9